AGU ADVANCING EARTH AND SPACE SCIENCE

Geophysical Research Letters®

The 28 November 2020 Landslide, Tsunami, and Outburst Flood – A Hazard Cascade Associated With Rapid Deglaciation at Elliot Creek, British Columbia, Canada

M. Geertsema[1,2] ⓘ, B. Menounos[2,3] ⓘ, G. Bullard[4], J. L. Carrivick[5] ⓘ, J. J. Clague[6] ⓘ, C. Dai[7] ⓘ, D. Donati[8] ⓘ, G. Ekstrom[9] ⓘ, J. M. Jackson[3] ⓘ, P. Lynett[10] ⓘ, M. Pichierri[11], A. Pon[11] ⓘ, D. H. Shugar[3,12] ⓘ, D. Stead[6], J. Del Bel Belluz[3], P. Friele[13], I. Giesbrecht[3] ⓘ, D. Heathfield[3], T. Millard[1] ⓘ, S. Nasonova[1], A. J. Schaeffer[14] ⓘ, B. C. Ward[6], D. Blaney[15], E. Blaney[16] ⓘ, C. Brillon[14], C. Bunn[17], W. Floyd[1,2,18], B. Higman[19], K. E. Hughes[1,20] ⓘ, W. McInnes[3] ⓘ, K. Mukherjee[21], and M. A. Sharp[12] ⓘ

[1]Ministry of Forests, Lands, Natural Resource Operations and Rural Development, Prince George, BC, Canada, [2]Geography, Earth and Environmental Sciences, University of Northern British Columbia, Prince George, BC, Canada, [3]Hakai Institute, Quadra Island, BC, Canada, [4]BGC Engineering Inc, Halifax, NS, Canada, [5]School of Geography and water@leeds, University of Leeds, Leeds, UK, [6]Department of Earth Sciences, Simon Fraser University, Burnaby, BC, Canada, [7]Department of Civil and Environmental Engineering, Louisiana State University, Baton Rouge, LA, USA, [8]Dipartimento di Ingegneria Civile, Chimica, Ambientale e dei Materiali, Alma Mater Studiorum - Università di Bologna, Bologna, Italy, [9]Lamont-Doherty Earth Observatory, Columbia University, Palisades, NY, USA, [10]Department of Civil and Environmental Engineering, University of Southern California, Los Angeles, CA, USA, [11]3vGeomatics Inc., Vancouver, BC, Canada, [12]Water, Sediment, Hazards, and Earth-surface Dynamics (waterSHED) Lab, Department of Geoscience, University of Calgary, Calgary, AB, Canada, [13]Cordilleran Geoscience, Squamish, BC, Canada, [14]Geological Survey of Canada, Pacific Division, Natural Resources Canada, Sidney, BC, Canada, [15]Homalco First Nation, Campbell River, BC, Canada, [16]Xwe'malkwhu First Nation, Powell River, BC, Canada, [17]Fisheries and Oceans, Campbell River, BC, Canada, [18]Department of Geography, Vancouver Island University, Nanaimo, BC, Canada, [19]Ground Truth Alaska, Seldovia, AK, USA, [20]Victoria University of Wellington, Wellington, NZ, [21]Cranfield University, Bedford, UK

Abstract We describe and model the evolution of a recent landslide, tsunami, outburst flood, and sediment plume in the southern Coast Mountains, British Columbia, Canada. On November 28, 2020, about 18 million m^3 of rock descended 1,000 m from a steep valley wall and traveled across the toe of a glacier before entering a 0.6 km^2 glacier lake and producing >100-m high run-up. Water overtopped the lake outlet and scoured a 10-km long channel before depositing debris on a 2-km^2 fan below the lake outlet. Floodwater, organic debris, and fine sediment entered a fjord where it produced a 60+km long sediment plume and altered turbidity, water temperature, and water chemistry for weeks. The outburst flood destroyed forest and salmon spawning habitat. Physically based models of the landslide, tsunami, and flood provide real-time simulations of the event and can improve understanding of similar hazard cascades and the risk they pose.

Plain Language Summary Glacier retreat exposes unstable slopes that can suddenly fail. We describe and model one such event with far-reaching consequences. The landslide mass (50 million tonnes, equivalent to the combined mass of all Canadian automobiles) entered and suddenly drained a 0.6-km^2 alpine lake in the southern Coast Mountains of British Columbia. Displaced water destroyed salmon-spawning habitat over a distance of 8.5 km and created a plume of sediment and organic matter more than 60 km from the head of the fjord into which the floodwaters discharged. Physically based models are able to simulate the hazard cascade, and such models could be used to improve hazard and risk assessments of these events under future climate change.

1. Introduction

Global glacier retreat is accelerating (Hugonnet et al., 2021). In high mountains, glacier shrinkage is destabilizing valley walls, leading to deep-seated gravitational movement, rockfalls, and rockslides (Cossart et al., 2008; Deline et al., 2021; Kos et al., 2016). In some settings, landslides that begin high on the flanks of mountains can transform into complex mass movements that trigger destructive and potentially deadly cascades of debris and water (Alford & Schuster, 2000; Chiarle et al., 2021; Evans et al., 2021; Hermanns et al., 2004, 2020; Hermanns, Dahle, et al., 2013; Hermanns, L'Heureux, et al., 2013; Hubbard et al., 2005; Shugar et al., 2021; Vilca et al., 2021).

The southern Coast Mountains of Western Canada contain over 8,000 km² of glacier-covered terrain (Bevington & Menounos, 2022; Bolch et al., 2010), and this region is currently experiencing some of the highest rates of glacier mass loss on Earth (Hugonnet et al., 2021; Menounos et al., 2019). Recent increases in rockslides and rock avalanches on massifs experiencing deglaciation, both in the Coast Mountains and elsewhere, attest to the association between glacier retreat and landslide frequency (Geertsema et al., 2006; Friele et al., 2020; Liu et al., 2021). Glacier retreat can also expose basins in which ice-contact or proglacial lakes form. Occasionally, these lakes fail catastrophically, generating extremely large floods (Veh et al., 2020), of which there are notable examples in British Columbia (Blown & Church, 1985; Clague & Evans, 2000). Although no landslide or outburst flood associated with recent glacier retreat in Western Canada has resulted in fatalities, notable increases in resource development, tourism, and municipal development will elevate the risk posed by these phenomena in the future.

In this study, we describe and model a recent landslide, tsunami, and outburst flood that occurred in recently deglaciated terrain within the traditional territory of the Homalco First Nation near the head of Bute Inlet, in the southern Coast Mountains of British Columbia (Figure 1). The landslide displaced water from a glacial lake and sent a torrent of water and debris down a salmon-bearing stream and into the ocean. We herein use the term tsunami to describe one or more waves that arise from a landslide entering a lake or fjord (e.g., Carey et al., 2012; Higman et al., 2018; Roberts et al., 2014). Our focus is on the terrestrial characteristics of the event, but we also briefly touch on the impacts to the marine environment of Bute Inlet. We describe the characteristics of the landslide source area, the movement of the failed rock mass, the landslide tsunami, the outburst flood down Elliot Creek, and some of the impacts in Bute Inlet. We also give an overview of the ecological impacts of the events on terrestrial and aquatic environments. Finally, we show that a physically based model can accurately simulate in real time the Elliot Creek event and thus could be applied in other glaciated mountain areas to better understand hazards and risks.

2. The Elliot Creek Landslide, Tsunami, Outburst Flood, and Sediment Plume

The event occurred in the Pacific Range of the British Columbia Coast Mountains, near the head of Elliot Creek, a tributary of the Southgate River (Figures 1 and 2). Local relief in the Elliot Creek watershed exceeds 1,600 m, and valley slopes are steep as a result of repeated Pleistocene glaciation. "Elliot Lake" (informal name) is a 2-km long, 350-m wide lake that formed during retreat of a valley glacier in the twentieth century (Figure 1). On November 28, 2020, a seismic event detector network recorded a landslide within 60 km of Elliot Creek, but its location was unclear until forestry workers discovered its aftermath some two weeks after the event.

2.1. The Landslide

Digital elevation model (DEM) analysis of lidar datasets acquired before and after the landslide reveal that 18.6 ± 0.34 (±2σ) million m³ of rock detached from a large body of weakly foliated quartz diorite with two prominent joint sets, one striking parallel to the slide flank and one striking parallel to the valley (Figure S2). Feature tracking using optical imagery methods (Dai et al., 2020) show that the pre-slide rock mass was moving horizontally at a rate of 0.4 ± 0.1 m yr⁻¹ (Figures S3 and S4). InSAR analysis indicates 15 cm of movement from June to October 2020 (Figures S5 and S6).

The main seismic signal produced by the landslide comprised long-period waves equivalent to a local $M \sim 5$ earthquake (Figures S7 and S8). In addition, a number of small earthquakes were recorded in the vicinity of Elliott Creek in the 6 hr preceding the slide (Figures S9 and S10). Post-event observations and subsequent modeling reveal that the slide mass moved nearly 1,000 m downslope in about 70 s. About 40% of the fragmented rock mass came to rest on the toe of the glacier above the lake. The remaining debris ran up the distal slope on the west side of the valley before entering the lake and creating a tsunami that exceeded 100 m in height. Using the approach proposed by Chow (1959), which equates potential to kinetic energy, and the highest observed landslide run-up (120 m), we obtain a peak and mean velocities of 48 and 34 m s⁻¹, respectively, for the slide mass that entered the lake.

The landslide followed a year of above-average precipitation (Figure S1). A precipitation event delivered 30–103 mm of rainfall in the week leading up to the landslide, with peak 24 hr precipitation of 10–58 mm at nearby low-elevation meteorological stations (Supporting Information SI). Higher elevation stations (1,481–1,574 m above sea level [m asl]) had snow cover of 52–125 cm, with mean temperatures below freezing for the
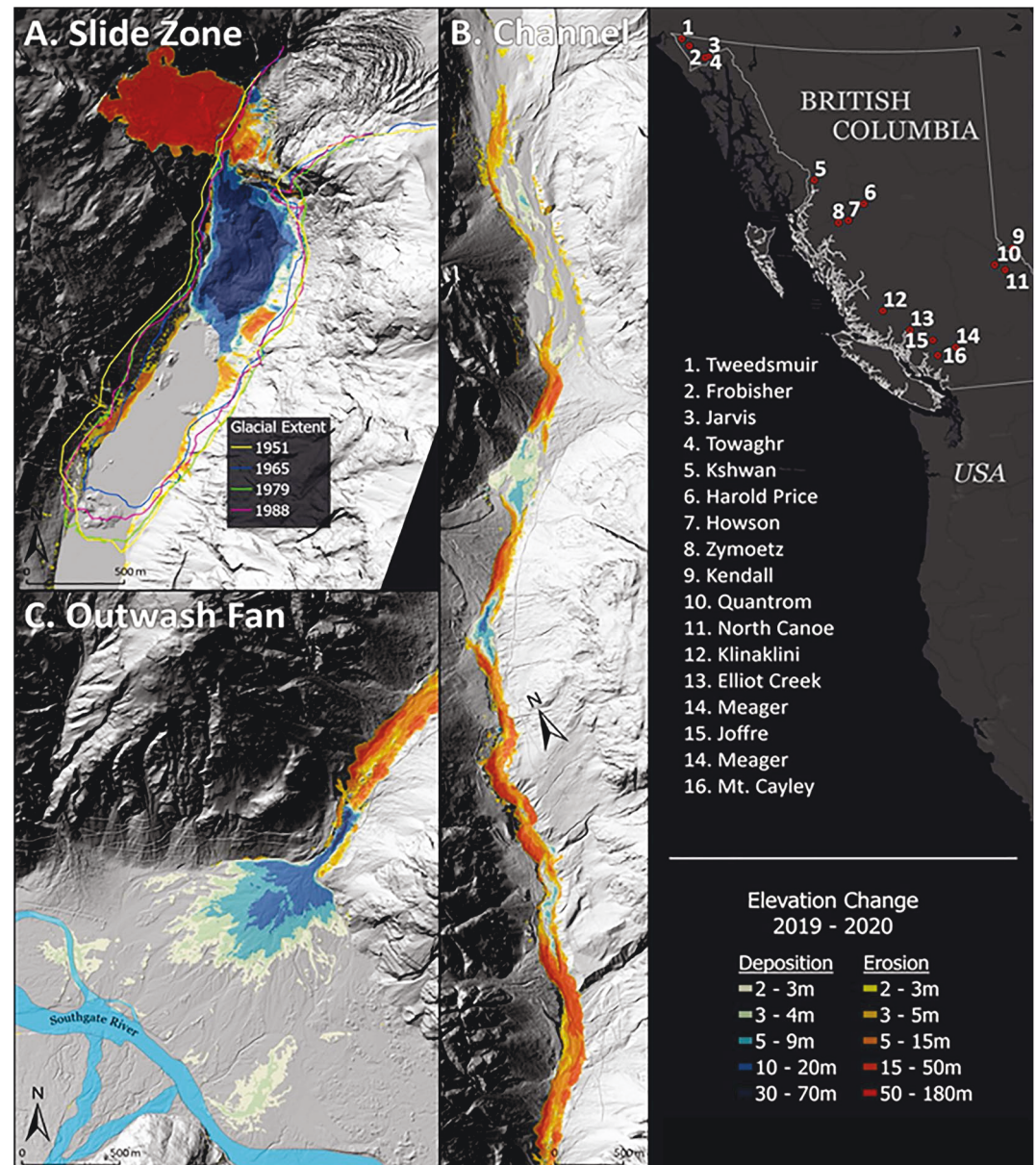
Figure 1. Map of study area. Panel (A): Lidar elevation difference map showing landslide source, or zone of depletion (red) and deposit, or zone of accumulation (blue) zones as well as glacier extents over time. Panels (B and C): Deposition and erosion by the outburst flood. Bottom right: The location of the Elliot Creek landslide and other landslides in glaciated areas in British Columbia (see Table S1).

duration of the event. Snowmelt may have contributed 10–30 mm of water to the rock mass in the landslide source area, but temperatures were near freezing in the lead-up to the failure.

The 2020 landslide was predated by an earlier, undated rockslide (Figures 2 and S2) that ran across a more extensive glacier sometime before 1951 (Figure 1).

2.2. Tsunami

Some 13.3 million m^3 of fragmented and bulked landslide debris traveled into the lake, forming several islands and reducing its area from 0.62 to 0.51 km^2. Sediment eroded from the shoreline by the push wave (as deep as
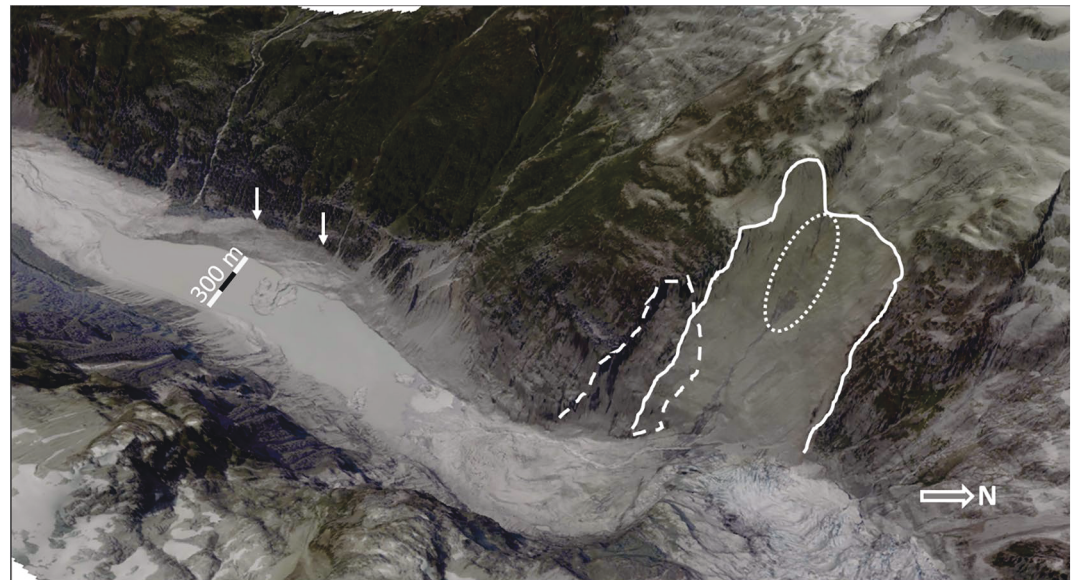
Figure 2. Oblique view of the November 28, 2020 rock avalanche (scarp solid white line) looking downstream into Elliot Lake and beyond into Elliot Creek. Note the trimline of the landslide-generated tsunami (white arrows) and flood that extends down valley. Note a previous rockslide (dashed white line) and the approximate zone of greatest preslide deformation detected from InSAR analysis in the year before failure (dotted white line).

12 m) contributed to lake filling. We estimate that approximately 15 million m^3 of water left Elliot Lake during the landslide and tsunami.

The tsunami produced a trimline on both sides of the lake (Figures 2 and 3). The run-up trimline on the west side of the lake reaches up to about 114 m above lake level, some 41 m higher than along its east side. Modeling of the slide and tsunami (Supporting Information) indicates the arrival of the slide mass at the lake within about 30 s (Figure 3). Numerical modeling indicates that the initial wave reached 72 m above the lake at its northeast end, close to the run-up observed in the satellite imagery (Figure 3; see animation at link under Data Availability Statement). The modeled leading wave traveled down the lake at speeds approaching 30 m s^{-1} and overtopped the lake outlet about 70 s after entering it. Our simulations show the subsequent arrival of reflected waves that are slower and smaller in amplitude (Supporting Information). The wave breaking limit, defined by Grilli et al. (1997) as a_m/h equals 0.78, where a_m is the difference between the wave crest and the water surface elevation and h is the maximum water depth, which was reached when the wave overtopped the moraine dam.

The outflow hydrograph, which we used as inflow into the downstream outburst flood model, was determined using a cross-section spanning the entire valley approximately 20 m south of Elliot Lake. The volume discharged by the leading wave is 12.0×10^6 m^3, and the total water discharged after accounting for all reflected waves is 13.5×10^6 m^3. Based on the pre-event surface topography, a lake volume loss of 13.5×10^6 m^3 would result in a reduction of 1.8 m in lake level. The discrepancy between the model and field estimates of lake water likely arises from uncertainty in pre-event lake volume and failure to account for sediment transport out of the lake basin. A wave overtopping the lake outlet with a peak flow of approximately 450,000 m^3 s^{-1} would also erode the crest of the dam, reducing its height and allowing for a larger volume to be released from the lake by the reflected waves. As a result, the breach hydrograph of the leading wave is considered to be a reasonable estimate.

2.3. Outburst Flood

We use the depth-integrated flow model COULWAVE (Kim et al., 2009) to simulate the flood dynamics immediately downstream of the lake. COULWAVE is typically used for coastal storm and tsunami investigations (e.g., Montoya & Lynett, 2018) and is applied here to capture the relatively small-scale behavior of the flooding wave. The flow model was initialized using the wave predicted by FLOW-3D with a spatial resolution of 3 m (Supporting Information). COULWAVE simulates the properties of the initial surge of the flood but does not include the
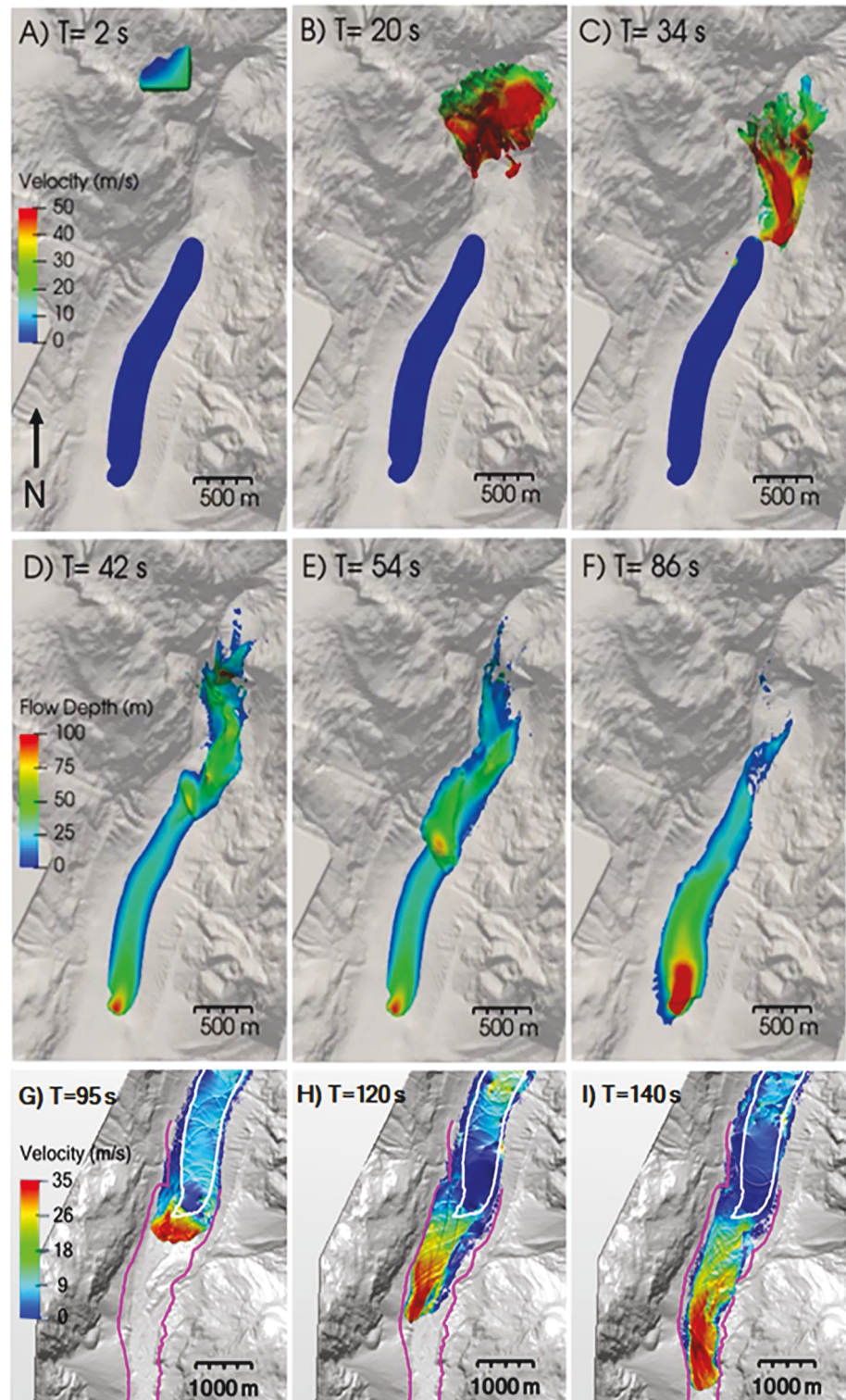
Figure 3. Summary of near-source numerical simulation results. FLOW-3D HYDRO model results for depth and velocity at six times: (a) 2, (b) 20, (c) 34, (d) 42, (e) 54, and (f) 86 s. Also shown COULWAVE model results for velocity at times: (g) 95, (h) 120, and (i) 140 s. All times are in seconds after release of the rock mass above Elliot Lake. The pre-slide lake shoreline is marked by the white contour, and the flood wash line by the magenta contour.
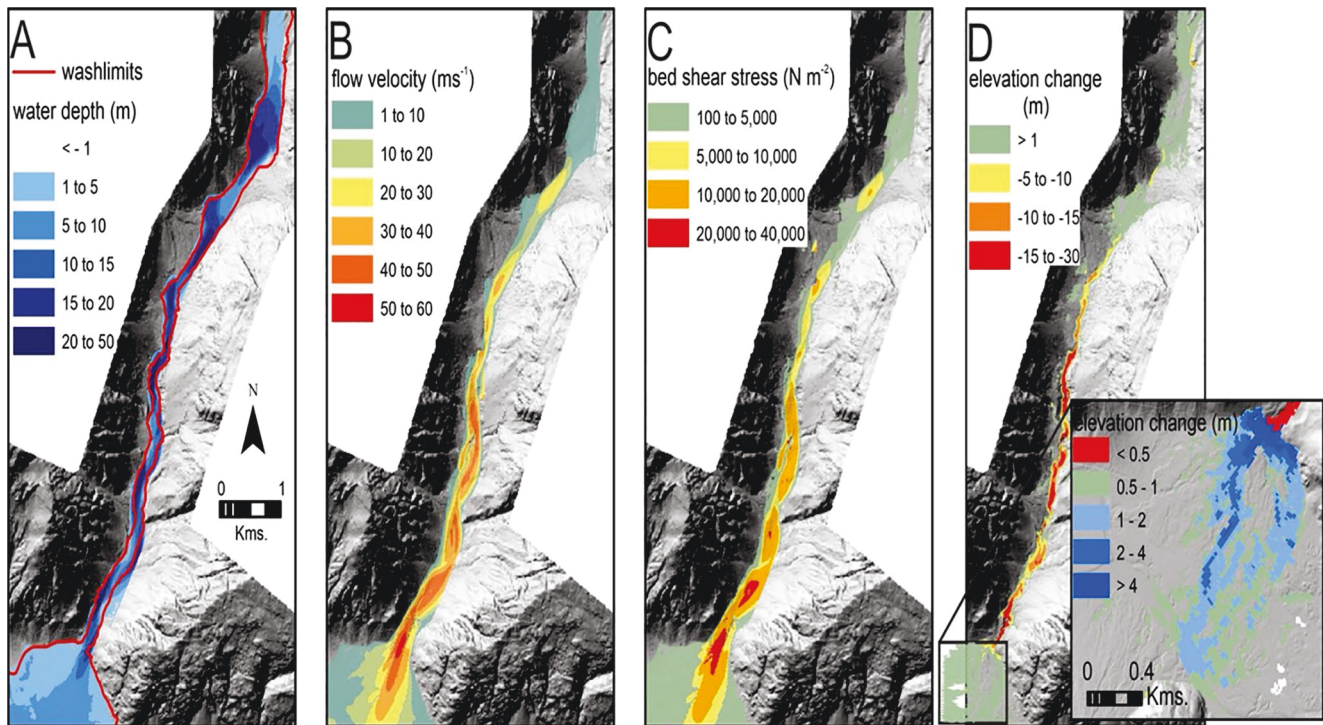
Figure 4. Modeled outburst flood (a) water depth, (b) flow velocity, (c) bed shear stress, and (d) sediment deposition, all 6 min after the moraine dam was breached. Inset in panel (D) is the fan after 20 min; note the different color scales.

effects of debris entrainment and topography alteration which, as described below, become increasingly important with distance downstream and duration of flooding.

COULWAVE-predicted flow velocities reveal the complexity of the flood (Figure 3). At 95 s post-slide (Figure 3g), the surge entirely overtopped the moraine dam, and the front of the flood was 200 m downstream of the lake outlet. At this time the flood was moving at a velocity of 35 m s^{-1} down the channel. Two minutes into the event (Figure 3h), the flood had traveled approximately 1.5 km from the lake; here there was a clear concentration of flow on the west side of the flooded area, driven by channel orientation. The modeling also reveals linear structures in the flow, which we interpret to be slowly moving short surface waves manifest as intense hydraulic jumps. After 140 s (Figure 3i), the flood had progressed another 800 m down the channel and maximum velocities were still in excess of 35 m s^{-1}. Predicted wash limits accord with observed data (Figure 1), indicating a reasonable hindcast of this complex event.

The flood wave traveled from the moraine dam to Bute Inlet in about 240 s, corresponding to an average frontal wave speed of 37.5 m s^{-1} (Figure 4). Predicted water depths averaged about 30 m along much of Elliot Creek, although water depths reached >50 m in bedrock-constrained reaches of the lower section of the creek (Figure 3). Estimated flow depths fell below 10 m after 12 min, except immediately upstream of several narrow gorges where hydraulic ponding occurred. and relatively deep water persisted up to 20 min after water left the lake.

Flow velocities in the main body of the outburst flood are modeled to have exceeded 60 m s^{-1}, but more typically were >30 m s^{-1} over most of the length of the valley. The highest flow velocities persisted through the 20-min duration of the falling limb/stage of the flood and were associated with the deepest parts of the flow within the central thalweg of the lower part of the valley. The model therefore suggests that the main body of the flow accelerated down the valley.

The flood in the upper reaches of Elliot Creek behaved as a Newtonian fluid but increasing bank failure and bed erosion provided sufficient sediment for the flood to transform into a non-Newtonian debris flood. The modeled outburst flood was supercritical (Froude number >1.0) along almost its entire route and for most of its 20-min duration. Sections where the flood was sub-critical are few and include a small topographic expansion about 2 km

down valley from the moraine dam, on the fan where Elliot Creek entered Southgate River, and along Southgate River between Elliot Creek and Bute Inlet. A hydraulic jump, marking a sharp transition between the supercritical and subcritical flow regimes, migrated up the fan during the flood. Bed shear stress likely exceeded 20,000 N m^{-2}. The greatest bed shear stress occurred between 6 and 20 min after flood onset as the main body of the flood propagated through the lower reaches of Elliot Creek.

The flood wave eroded and deposited sediment along Elliot Creek (Figure 1). Modeled bed elevation change is dominated by erosion, but some infilling occurred in the upper part of the valley immediately downstream of the moraine dam, on the preexisting floodplain and terraces, in some small topographic expansions in the lower gorge part of the valley, and especially on the fan at the mouth of the valley. A complex pattern of minor erosion and deposition is modeled to have occurred along the flanks of the lower part of the valley above the gorge walls. In some sections where the flow was constrained, the channel floor was deepened more than 40 m.

Sequential DEM analysis reveals that the channel lost $8.31 \pm 2.39 \times 10^6$ m^3 of sediment between the lake outlet and the fan apex (Figure 1). Of this amount, $3.95 \pm 2.85 \times 10^6$ m^3 of sediment up to 5-m thick was deposited on the fan, and the remaining 4.36×10^6 m^3 was transported down Southgate River and into Bute Inlet. Deposition on the fan and the introduction of coarse woody debris into Southgate River briefly dammed the river, raising its level about 3 m.

The tsunami and flood destroyed about 3 km^2 of forest. Additionally, some 3.5 km of Coho and Chinook spawning habitat were damaged in lower Elliot Creek, and about 5 km of Chum salmon spawning habitat in Southgate River were negatively impacted by deposition of fine sediment. Continued stream avulsions on the Elliot Creek fan limit remediation of fish habitat.

2.4. Sediment Plume

The event delivered water, sediment, and organic debris to the marine environment in Bute Inlet. About 4 million m^3 of sediment eroded from Elliot Creek entered Southgate River, and some of this sediment was carried more than 60 km down Bute Inlet. The influx of 15×10^6 m^3 of freshwater from the outburst flood also changed the water temperature, salinity, and oxygen levels in the inlet (Figure 5). The largest changes occurred in waters deeper than 200 m. From October 22, 2020, to December 2, 2020, turbidity increased by about 200% (from 2 to 6 NTUs) between 250 and 600 m depth. A 70-year observation record (Jackson, Bianucci, et al., 2021; Jackson, Johannessen, et al., 2021) shows that water temperature cooled from 9.6° to 9.1°C, changing the long-term warming trend of 1.3°C over this period. Salinity freshened by 0.05, from 30.88 to 30.83, changing the long-term salinification trend of 0.2 salinity units over 70 years. Oxygen increased 0.36 ml L^{-1}, from 2.21 to 2.57 ml L^{-1}, changing the long-term deoxygenation trend of 0.6 ml L^{-1} over 70 years.

3. Discussion

The trigger for the Elliot Creek landslide is unknown, but factors that led to the failure include fractured bedrock with favorably oriented joints and debuttressing of the base of the slope due to glacier retreat. A gradual reduction in normal stress at the toe of the slope and progressive fatigue of the rock mass, concentrated along fractures, decreased the overall stability of the slope over the past century. We expect that permafrost degradation, important in many mountain landslides (Deline et al., 2021; Huggel et al., 2012), did not play a role here according to available gridded models that combine altitude, slope, aspect, air temperature, and potential incoming solar radiation (Gruber, 2012; Hasler & Geertsema, 2013). An older landslide scar that is visible in aerial photography reveals that a landslide occurred from the same location before the 1950s. The older landslide likely ran across the glacier before Elliot Lake formed and thus the catastrophic flood experienced during the recent event could not have occurred.

The Elliot Creek event is an example of a, sometimes underappreciated, hazard chain in high mountains experiencing rapid deglaciation. This event finds itself among other disastrous high mountain landslides that generate tsunami (Higman et al., 2018; Roberts et al., 2014) and floods and fast-moving mass flows (Carey et al., 2012; Glancy & Bell, 2000; Franco et al., 2021; Hermanns et al., 2004; Hermanns, Dahle, et al., 2013; Hermanns, L'Heureux, et al., 2013; Hubbard et al., 2005; Oppikofer et al., 2012; Shugar, Jacquemart, et al., 2021; Vilca et al., 2021). Rapid glacier retreat may increase the hazard of these events as the number and size of lakes increase
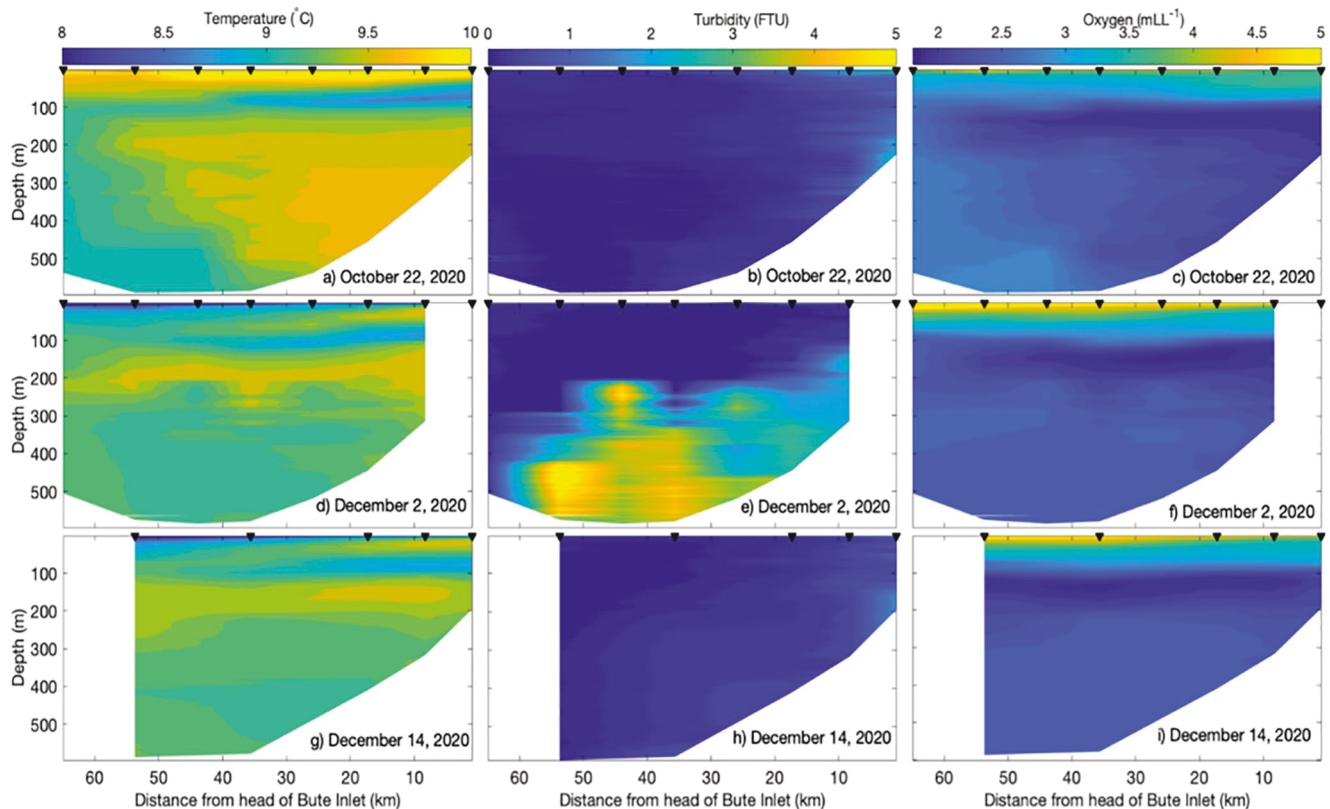
Figure 5. (Left column) temperature, (middle column) turbidity, and (right column) oxygen of the Bute Inlet water column (top row) before, (middle row) 4 days after, and (bottom row) 16 days after the Elliott Creek landslide. Contour plots are oriented so that the head of Bute Inlet is on the right and the mouth of Bute Inlet is on the left. Black triangles indicate station locations. Note that not all eight stations were sampled on December 2 or December 14.

below potentially unstable slopes in alpine valleys undergoing ice retreat. Even small landslides or ice avalanches into existing and newly formed lakes can displace enough water to induce downstream floods large enough to cause serious damage and injury (Clague & Evans, 2000).

More than 1,000 glacier lake outburst floods from alpine lakes have been reported globally since 1900 CE, resulting in more than 12,500 fatalities, with large amounts of damage to infrastructure and farmland, and disruptions of transportation and communication (Carrivick & Tweed, 2016). Not all GLOFs are triggered by landslides or avalanches, but most, like the Elliot Creek event, involve complex down valley flows varying in time and space from clearwater floods through hyperconcentrated and debris flows (Clague & Evans, 2000; Clague & O'Connor, 2021). In that sense, they are examples of hazard cascades, in which a triggering event produces an outflow that commonly evolves and causes secondary effects as it propagates down valley (Hermanns et al., 2004; Kirschbaum et al., 2019; Worni et al., 2014). An assessment of the hazard posed by landslides and avalanches into alpine lakes requires lake inventories and modeling that can help predict where and why these lakes will form and grow in the future (e.g., Haeberli et al., 2017; Haeberli & Drenkhan, 2022; Oppikofer et al., 2019; Shugar, Burr, et al., 2021; Veh et al., 2020;), as well as the likely behavior of outflowing waters in the event of landslide-triggered tsunami.

The Elliot valley event is by no means the first such event in British Columbia. Notable examples of large outburst floods resulting from ice avalanches into young moraine-dammed lakes include well document events at Klattasine Creek (early 1970s; Clague et al., 1985), Nostetuko (1984; Blown & Church, 1985), and Queen Bess (1997; Kershaw et al., 2005), all within 40 km of Elliot Lake (Figure 1). Fortunately, these and other similar events in Western Canada have occurred in remote mountain valleys and have not been lethal. However, there is no assurance that this will be true in the future, given increased development and tourism in these formerly remote areas.

Agreement between our physically based modeling of the Elliot Creek event and field evidence of suggests that such models can be adapted for outburst flood prediction. Further, surface inversion techniques for predicting topography below current glaciers (Farinotti et al., 2019) have evolved to allow mapping of future lake locations (Zheng et al., 2021). Combining these data with existing (Clarke et al., 2015) and new (Edwards et al., 2021) glacier evolution projections will allow researchers to assess recently exposed lakes (Mölg et al., 2021; Shugar, Burr, et al., 2021) and model future lakes as they develop throughout the remainder of this century. Modeled and measured permafrost degradation and debuttressing data could be used to classify dangerous slopes (e.g., Allen et al., 2022; Deline et al., 2021; Haeberli et al., 2017). Existing and new sites of lake formation could then be combined with topographic, geologic, and development data and incorporated into state-of-the-art physical models to improve hazard and risk assessments in western Canada and elsewhere.

The Elliot Creek event impacted terrestrial, riverine, and marine environments. It destroyed key salmon spawning habitats in Southgate River and lower Elliot Creek. These habitats provide important food sources for the Homalco First Nations. The landslide itself impacted a relatively small area (about 1 km^2), but the tsunami and outburst flood destroyed some 3 km^2 of forest and removed and buried soil along their paths. Subaerial landslide sediment plumes (Hughes et al., 2021), though not widely studied, may influence marine ecosystems such as kelp forests (Kiest, 1993). Although, as mentioned above, landslides and outburst floods have happened in these mountains for millennia, salmon are now experiencing low returns due to a complex set of factors, including atmospheric warming and habitat degradation.

Data Availability Statement

Lidar data and landslide, tsunami, and flood animations are available here: https://datadryad.org/stash/share/VSj-5T1v0_enwOhlalauFxAD1J16ZPJWeKPIz3vXQ90. ERA5 data is obtained from Hershbach and Dee (2016).

References

Alford, D., & Schuster, R. L. (2000). *Usoi landslide dam and Lake Sarez*. United Nations Publications, ISDR Prevention Series, v. Book, 113 p.

Allen, S., Frey, H., Haeberli, W., Huggel, C., Chiarle, M., & Geertsema, M. (2022). Assessment principles for glacier and permafrost hazards in mountain regions. In *Natural hazard science*. Oxford University Press. https://doi.org/10.1093/acrefore/9780199389407.013.356

Bevington, A., & Menounos, B. (2022). Accelerated change in the glaciated environments of western Canada revealed through trend analysis of optical satellite imagery. *Remote Sensing of Environment*, *270*, 112862. https://doi.org/10.1016/j.rse.2021.112862

Blown, I., & Church, M. (1985). Catastrophic lake drainage within the Homathko River basin, British Columbia. *Canadian Geotechnical Journal*, *22*(4), 551–563. https://doi.org/10.1139/t85-075

Bolch, T., Menounos, B., & Wheate, R. (2010). Landsat-based inventory of glaciers in western Canada, 1985–2005. *Remote Sensing of Environment*, *114*(1), 127–137. https://doi.org/10.1016/j.rse.2009.08.015

Carey, M., Huggel, C., Bury, J., Portocarrero, C., & Haeberli, W. (2012). An integrated socio-environmental framework for glacier hazard management and climate change adaptation: Lessons from Lake 513, Cordillera Blanca, Peru. *Climatic Change*, *112*(3), 733–767. https://doi.org/10.1007/s10584-011-0249-8

Carrivick, J. L., & Tweed, F. S. (2016). A global assessment of the societal impacts of glacier outburst floods. *Global and Planetary Change*, *144*, 1–16. https://doi.org/10.1016/j.gloplacha.2016.07.001

Chiarle, M., Geertsema, M., Mortara, G., & Clague, J. J. (2021). Relations between climate change and mass movement: Perspectives from the Canadian Cordillera and the European Alps. *Global and Planetary Change*, *202*, 103499. https://doi.org/10.1016/j.gloplacha.2021.103499

Chow, V. T. (1959). *Open channel Hydraulics*. McGraw-Hill.

Clague, J. J., & Evans, S. G. (2000). A review of catastrophic drainage of moraine-dammed lakes in British Columbia. *Quaternary Science Reviews*, *19*(17–18), 1763–1783. https://doi.org/10.1016/s0277-3791(00)00090-1

Clague, J. J., Evans, S. G., & Blown, I. G. (1985). A debris flow triggered by the breaching of a moraine-dammed lake, Klattasine Creek, British Columbia. *Canadian Journal of Earth Sciences*, *22*, 1492–1502. https://doi.org/10.1139/e85-155

Clague, J. J., & O'Connor, J. E. (2021). Glacier-related outburst floods. In W. Haeberli & C. Whiteman (Eds.), *Snow and ice-related hazards, risks, and disasters* (pp. 467–499). Elsevier. https://doi.org/10.1016/b978-0-12-817129-5.00019-6

Clarke, G. K. C., Jarosch, A. H., Anslow, F. S., Radić, V., & Menounos, B. (2015). Projected deglaciation of western Canada in the twenty-first century. *Nature Geoscience*, *8*(5), 372–377. https://doi.org/10.1038/ngeo2407

Cossart, E., Braucher, R., Fort, M., Bourlès, D. L., & Carcaillet, J. (2008). Slope instability in relation to glacial debuttressing in alpine areas (Upper Durance catchment, southeastern France): Evidence from field data and 10Be cosmic ray exposure ages. *Geomorphology*. https://doi.org/10.1016/j.geomorph.2006.12.022

Deline, P., Gruber, S., Amann, F., Bodin, X., Delaloye, R., Failletaz, J., et al. (2021). Ice loss from glaciers and permafrost and related slope instability in high-mountain regions. In W. Haeberli & C. Whiteman (Eds.), *Snow and ice-related hazards, risks, and disasters* (pp. 501–540). Elsevier. https://doi.org/10.1016/b978-0-12-817129-5.00015-9

Edwards, T. L., Nowicki, S., Marzeion, B., Hock, R., Goelzer, H., & Seroussi, H. (2021). Projected land ice contributions to twenty-first-century sea level rise. *Nature*, *593*(7857), 74–82.

Evans, S. G., Bishop, N. F., Smoll, L. F., Murillo, P. V., Delaney, K. B., & Oliver-Smith, A. (2009). A re-examination of the mechanism and human impact of catastrophic mass flows originating on Nevado Huascarán, Cordillera Blanca, Peru in 1962 and 1970. *Engineering Geology*. https://doi.org/10.1016/j.enggeo.2009.06.020

Evans, S. G., Delaney, K. B., & Rana, N. M. (2021). The occurrence and mechanism of catastrophic mass flows in the mountain cryosphere. In W. Haeberli & C. Whiteman (Eds.), *Snow and ice-related hazards, risks, and disasters* (pp. 541–596). Elsevier. https://doi.org/10.1016/b978-0-12-817129-5.00004-4

Farinotti, D., Huss, M., Fürst, J. J., Landmann, J., Machguth, H., Maussion, F., & Pandit, A. (2019). A consensus estimate for the ice thickness distribution of all glaciers on Earth. *Nature Geoscience*, *12*(3), 168–173. https://doi.org/10.1038/s41561-019-0300-3

Franco, A., Schneider-Muntau, B., Roberts, N. J., Clague, J. J., & Gems, B. (2021). Geometry-based preliminary quantification of landslide-induced impulse wave attenuation in mountain lakes. *Applied Sciences*, *11*(24), 11614. https://doi.org/10.3390/app112411614

Friele, P., Millard, T. H., Mitchell, A., Allstadt, K. E., Menounos, B., Geertsema, M., & Clague, J. J. (2020). Observations on the May 2019 Joffre Peak landslides, British Columbia. *Landslides*, *17*(4), 913–930. https://doi.org/10.1007/s10346-019-01332-2

Geertsema, M., Clague, J. J., Schwab, J. W., & Evans, S. G. (2006). An overview of recent large catastrophic landslides in northern British Columbia, Canada. *Engineering Geology*, *83*(1–3), 120–143.

Glancy, P. A., & Bell, J. W. (2000). *Landslide-induced flooding at Ophir Creek, Washoe County, western Nevada, May 30, 1983*. U.S. Geological Survey Professional Paper, 1617, pp. 1–94.

Grilli, S. T., Svendsen, I. A. & Subramanya, R. (1997). Breaking criterion and characteristics for solitary waves on slopes. *Journal of waterway, port, coastal, and ocean engineering*, *123*(3), 102–112.

Gruber, S. (2012). Derivation and analysis of a high-resolution estimate of global permafrost zonation. *The Cryosphere*, *6*(1), 221–233. https://doi.org/10.5194/tc-6-221-2012

Haeberli, W., & Drenkhan, F. (2022). Future lake development in deglaciating mountain ranges. *Oxford Research Encyclopedia on Natural Hazard Science*.

Haeberli, W., Schaub, Y., & Huggel, C. (2017). Increasing risks related to landslides from degrading permafrost into new lakes in de-glaciating mountain ranges. *Geomorphology*, *293*, 405–417. https://doi.org/10.1016/j.geomorph.2016.02.009

Hasler, A., & Geertsema, M. (2013). *Provisional permafrost map of British Columbia*. Retrieved from http://www.env.gov.bc.ca/esd/distdata/ecosystems/PermaFrostModel/

Hermanns, R. L., Dahle, H., Bjerke, P. L., Crosta, G. B., Anda, E., Blikra, L. H., et al. (2013). Rockslide dams in Møre og Romsdal County, Norway. In C. Margottini, P. Canuti, & K. Sassa (Eds.), *Landslide science and practice* (pp. 3–12). Springer Berlin Heidelberg. https://doi.org/10.1007/978-3-642-31319-6_1

Hermanns, R. L., L'Heureux, J. S., & Blikra, L. H. (2013). Landslide triggered tsunami, displacement wave. In P. T. Bobrowsky (Ed.), *Encyclopedia of natural hazards. Encyclopedia of Earth Sciences Series*. Springer. https://doi.org/10.1007/978-1-4020-4399-4_95

Hermanns, R. L., Niedermann, S., Ivy, O., & Kubik, P. W. (2004). Rock avalanching into a landslide-dammed lake causing multiple dam failure in Las Conchas valley (NW Argentina)—Evidence from surface exposure dating and stratigraphic analyses. *Landslides*, *1*(2), 113–122. https://doi.org/10.1007/s10346-004-0013-5

Hermanns, R. L., Oppikofer, T., Böhme, M., Penna, I. M., Nicolet, P., & Bredal, M. (2020). Mapping, hazard and consequence analyses for unstable rock slopes in Norway. In *Proceedings Workshop on World Landslide Forum 2020* (pp. 317–323). Springer. https://doi.org/10.1007/978-3-030-60713-5_29

Higman, B., Shugar, D. H., Stark, C. P., Ekström, G., Koppes, M. N., Lynett, P., et al. (2018). The 2015 landslide and tsunami in Taan Fiord, Alaska. *Scientific Reports*, *8*(1), 1–12. https://doi.org/10.1038/s41598-018-30475-w

Hubbard, B., Heald, A., Reynolds, J. M., Quincey, D., Richardson, S. D., Luyo, M. Z., & Hambrey, M. J. (2005). Impact of a rock avalanche on a moraine-dammed proglacial lake: Laguna Safuna Alta, Cordillera Blanca, Peru. *Earth Surface Processes and Landforms*, *30*(10), 1251–1264. https://doi.org/10.1002/esp.1198

Huggel, C., Clague, J. J., & Korup, O. (2012). Is climate change responsible for changing landslide activity in high mountains? *Earth Surface Processes and Landforms*, *37*, 77–91. https://doi.org/10.1002/esp.2223

Hughes, K. E., Wild, A., Kwoll, E., Geertsema, M., Perry, A., & Harrison, K. D. (2021). Remote sensing of landslide-generated sediment plumes, Peace River, British Columbia. *Remote Sensing*, *13*(23), 4901. https://doi.org/10.3390/rs13234901

Hugonnet, R., McNabb, R., Berthier, E., Menounos, B., Nuth, C., Girod, L., et al. (2021). Accelerated global glacier mass loss in the early twenty-first century. *Nature*, *592*(7856), 726–731. https://doi.org/10.1038/s41586-021-03436-z

Jackson, J. M., Bianucci, L., Hannah, C. G., Carmack, E. C., & Barrette, J. (2021). Deep waters in British Columbia mainland fjords show rapid warming and deoxygenation from 1951 to 2020. *Geophysical Research Letters*, *48*, e2020GL091094. https://doi.org/10.1029/2020gl091094

Jackson, J. M., Johannessen, S., Del Del Belluz, J., Hunt, B. P. V., & Hannah, C. G. (2021). Identification of a seasonal subsurface oxygen minimum in Rivers Inlet, British Columbia. *Estuaries and Coasts*, 1–18.

Kershaw, J. A., Clague, J. J., & Evans, S. G. (2005). Geomorphological and sedimentological signature of a two-phase outburst flood from moraine=dammed Queen Bess Lake, British Columbia, Canada. *Earth Surface Processes and Landforms*, *30*, 1–25. https://doi.org/10.1002/esp.1122

Kiest, K. A. (1993). *The influence of sediment from landslide plumes on sessile kelp forest assemblages* (Doctoral dissertation). San Jose State University.

Kim, D. H., Lynett, P. J., & Socolofsky, S. A. (2009). A depth-integrated model for weakly dispersive, turbulent, and rotational fluid flows. *Ocean Modelling*, *27*(3–4), 198–214. https://doi.org/10.1016/j.ocemod.2009.01.005

Kirschbaum, D. L., Watson, C. S., Rounce, D. R., Shugar, D. H., Kargel, J .S., Haritashya, U. K., et al. (2019). Remote sensing of cascading hazards over High Mountain Asia. *Frontiers of Earth Science*, *7*, 197. https://doi.org/10.3389/feart.2019.00197

Kos, A., Amann, F., Strozzi, T., Delaloye, R., von Ruette, J., & Springman, S. (2016). Contemporary glacier retreat triggers a rapid landslide response, Great Aletsch Glacier, Switzerland. *Geophysical Research Letters*, *43*(24), 2016GL071708. https://doi.org/10.1002/2016gl071708

Liu, J., Wu, Y., & Gao, X. (2021). Increase in occurrence of large glacier-related landslides in the high mountains of Asia. *Scientific Reports*, *11*(1), 1635. https://doi.org/10.1038/s41598-021-81212-9

Menounos, B., Hugonnet, R., Shean, D., Gardner, A., Howat, I., Berthier, E., et al. (2019). Heterogeneous changes in western North American glaciers linked to decadal variability in zonal wind strength. *Geophysical Research Letters*, *46*(1), 200–209. https://doi.org/10.1029/2018gl080942

Mölg, N., Huggel, C., Herold, T., Storck, F., Allen, S., Haeberli, W., et al. (2021). Inventory and evolution of glacial lakes since the Little Ice Age: Lessons from the case of Switzerland. *Earth Surface Processes and Landforms*, *46*(13), 2551–2564.

Montoya, L., & Lynett, P. (2018). Tsunami versus infragravity surge comparison of the physical character of extreme runup. *Geophysical Research Letters*, *45*(23), 12–982. https://doi.org/10.1029/2018gl080594

Oppikofer, T., Hermanns, R. L., Redfield, T. F., Sepúlveda, S. A., Duhart, P., & Bascuñán, I. (2012). Morphologic description of the Punta Cola rock avalanche and associated minor rockslides caused by the 21 April 2007 Aysén earthquake (Patagonia, southern Chile). *Revista de la Asociación Geológica Argentina*, *69*(3), 339–353.

Oppikofer, T., Hermanns, R. L., Roberts, N. J., & Böhme, M. (2019). SPLASH: Semi-empirical prediction of landslide-generated displacement wave run-up heights. *Geological Society, London, Special Publications*, *477*(1), 353–366. https://doi.org/10.1144/sp477.1

Roberts, N. J., McKillop, R., Hermanns, R. L., Clague, J. J., & Oppikofer, T. (2014). Preliminary global catalogue of displacement waves from subaerial landslides. In *Landslide science for a safer geoenvironment* (pp. 687–692). Springer. https://doi.org/10.1007/978-3-319-04996-0_104

Shugar, D. H., Burr, A., Haritashya, U. K., Kargel, J. S., Scott Watson, C., Kennedy, M. C., et al. (2021). Rapid worldwide growth of glacial lakes since 1990. *Nature Climate Change*, *10*(10), 939–945.

Shugar, D. H., Jacquemart, M., Shean, D., Bhushan, S., Upadhyay, K., Sattar, A., et al. (2021). A massive rock and ice avalanche caused the 2021 disaster at Chamoli, Indian Himalaya. *Science*, *373*(6552), 300–306. https://doi.org/10.1126/science.abh4455

Veh, G., Korup, O., & Walz, A. (2020). Hazard from Himalayan glacier lake outburst floods. *Proceedings of the National Academy of Sciences of the United States of America*, *117*(2), 907–912. https://doi.org/10.1073/pnas.1914898117

Vilca, O., Mergili, M., Emmer, A., Frey, H., & Huggel, C. (2021). The 2020 glacial lake outburst flood process chain at Lake Salkantaycocha (Cordillera Vilcabamba, Peru). *Landslides*, *18*, 2211–2223. https://doi.org/10.1007/s10346-021-01670-0

Worni, R., Huggel, C., Clague, J. J., Schaub, Y., & Stoffel, M. (2014). Coupling glacial lake impact, dam breach, and flood processes: A modeling perspective. *Geomorphology*, *224*, 161–176. https://doi.org/10.1016/j.geomorph.2014.06.031

Zheng, G., Allen, S. K., Bao, A., Ballesteros-Cánovas, J. A., Huss, M., Zhang, G., et al. (2021). Increasing risk of glacial lake outburst floods from future Third Pole deglaciation. *Nature Climate Change*, *11*(5), 411–417. https://doi.org/10.1038/s41558-021-01028-3

References From the Supporting Information

Carrivick, J. (2009). In D. M. Burr, P. A. Carling & V. R. Baker (Eds.), *Jökulhlaups from Kverkfjöll volcano, Iceland: Modelling transient hydraulic phenomena* (pp. 273–289). Cambridge University Press.

Carrivick, J. L., Brown, L. E., Hannah, D. M., & Turner, A. G. D. (2012). Numerical modelling of spatio-temporal thermal heterogeneity in a complex river system. *Journal of Hydrology*, *414*, 491–502. https://doi.org/10.1016/j.jhydrol.2011.11.026

Carrivick, J. L., Manville, V., & Cronin, S. J. (2009). A fluid dynamics approach to modelling the 18th March 2007 lahar at Mt. Ruapehu, New Zealand. *Bulletin of Volcanology*, *71*, 153–169. https://doi.org/10.1007/s00445-008-0213-2

Carrivick, J. L., Manville, V., Graettinger, A., & Cronin, S. J. (2010). Coupled fluid dynamics-sediment transport modelling of a Crater Lake break-out lahar: Mt. Ruapehu, New Zealand. *Journal of Hydrology*, *388*(3), 399–413. https://doi.org/10.1016/j.jhydrol.2010.05.023

Carrivick, J. L., Turner, A. G. D., Russell, A. J., Ingeman-Nielsen, T., & Yde, J. C. (2013). Outburst flood evolution at Russell Glacier, western Greenland: Effects of a bedrock channel cascade with intermediary lakes. *Quaternary Science Reviews*, *67*, 39–58. https://doi.org/10.1016/j.quascirev.2013.01.023

CloudCompare. (2019). CloudCompare (Version 2.12). [Software]. CloudCompare. Retrieved from http://www.cloudcompare.org/

Cruden, D. M., & Lu, Z.-Y. (1992). The rockslide and debris flow at Mt. Cayley, BC, in June 1984. *Canadian Geotechnical Journal*, *29*(4), 614–626.

Dai, C., Higman, B., Lynett, P. J., Jacquemart, M., Howat, I. M., Liljedahl, A. K., et al. (2020). Detection and assessment of a large and potentially Tsunamigenic Periglacial Landslide in Barry Arm, Alaska. *Geophysical Research Letters*, *47*, e2020GL089800. https://doi.org/10.1029/2020GL089800

Ekström, G. (2006). Global detection and location of seismic sources by using surface waves. *Bulletin of the Seismological Society of America*, *96*(4A), 201–212. https://doi.org/10.1785/0120050175

Ekström, G., & Stark, C. P. (2013). Simple scaling of catastrophic landslide dynamics. *Science*, *339*, 1416–1419. https://doi.org/10.1126/science.1232887

Ersoy, H., Karahan, M., Gelişli, K., Akgün, A., Anılan, T., Sünnetci, M. O., et al. (2019). Modelling of the landslide-induced impulse waves in the Artvin Dam reservoir by empirical approach and 3D numerical simulation. *Engineering Geology*, *249*, 112–128.

ESRI. (2019). ArcGIS Desktop (Release 10). [Software]. *Environmental Systems Research Institute*. .

Flow Science. (2020). Flow-3D (Version 12.0). [Software]. *Flow Science, Inc*. https://www.flow3d.com

Franco, A., Moernaut, J., Schneider-Muntau, B., Strasser, M., & Gems, B. (2020). The 1958 Lituya Bay tsunami–pre-event bathymetry reconstruction and 3D numerical modelling utilising the computational fluid dynamics software Flow-3D. *Natural Hazards and Earth System Sciences*, *20*, 2255–2279.

Geertsema, M., & Bevington, A. (2021). A cautionary note for rock avalanche field investigation: Recent sequential and overlapping landslides in British Columbia. *Canadian Geotechnical Journal*, *58*(5), 737–740. https://doi.org/10.1139/cgj-2019-0751

Hershbach, H., & Dee, D. (2016). ERA5 reanalysis is in production. *ECMWF Newsletter*, *147*, 7.

Hibert, C., Stark, C. P., & Ekström, G. (2015). Dynamics of the Oso-Steelhead landslide from broadband seismic analysis. *Natural Hazards and Earth System Sciences*, *15*(6), 1265–1273. https://doi.org/10.5194/nhess-15-1265-2015

Hirt, C. W., & Nichols, B. D. (1981). Volume of fluid (VOF) method for the dynamics of free boundaries. *Journal of Computational Physics*, *39*(1), 201–225. https://doi.org/10.1016/0021-9991(81)90145-5

Jackson, J. M., Allen, S. E., Carmack, E. C., & McLaughlin, F. J. (2010). Suspended particles in the Canada Basin from optical and bottle data, 2003-2008. *Ocean Science*, *6*, 799–813. https://doi.org/10.5194/os-6-799-2010

Keefer, D. K. (1984). Landslides caused by earthquakes. *The Geological Society of America Bulletin*, *95*(4), 406–421. https://doi.org/10.1130/0016-7606

Keefer, D. K. (2002). Investigating landslides caused by earthquakes—A historical review. *Surveys in Geophysics*, *23*(6), 473–510. https://doi.org/10.1023/A:1021274710840

Kim, G. B., Cheng, W., Sunny, R. C., Horrillo, J. J., McFall, B. C., Mohammed, F., et al. (2019). Three dimensional landslide generated tsunamis: Numerical and physical model comparisons. *Landslides*, 1–17.

Leprince, S., Ayoub, F., Klinger, Y., & Avouac, J. P. (2007). *Co-registration of optically sensed images and correlation (COSI-Corr): An operational methodology for ground deformation measurements*. Paper presented at the 2007 IEEE International Geoscience and Remote Sensing Symposium (pp. 1943–1946). IEEE.

Lesser, G. R., Roelvink, J. V., van Kester, J. T. M., & Stelling, G. S. (2004). Development and validation of a three-dimensional morphological model. *Coastal Engineering*, *51*(8–9), 883–915. https://doi.org/10.1016/j.coastaleng.2004.07.014

Lu, Z. Y., & Cruden, D. M. (1996). Two debris flow modes on Mount Cayley, British Columbia. *Canadian Geotechnical Journal*, *33*(1), 123–139. https://doi.org/10.1139/t96-028

Martino, S., Bozzano, F., Caporossi, P., D'Angio, D., Della Seta, M., Esposito, C., et al. (2019). Impact of landslides on transportation routes during the 2016-2017 Central Italy seismic sequence. *Landslides*, *16*, 1221–1241. https://doi.org/10.1007/s10346-019-01162-2

Meyer-Peter, E., & Müller, R. (1948). Formulas for bed load transport. Paper presented at 2nd Meeting International Association for Hydro-Environment Engineering and Research.

Nuth, C., & Kaab, A. (2011). Co-registration and bias corrections of satellite elevation data sets for quantifying glacier thickness change. *The Cryosphere*, *5*(1), 271–290.

RGI Consortium. (2017). *Randolph glacier inventory—A dataset of global glacier outlines (version 6.0)*. Global Land Ice Measurements from Space. https://doi.org/10.7265/N5-RGI-60

Roberti, G., Ward, B., de Vries, B. V. W., Friele, P., Perotti, L., Clague, J. J., & Giardino, M. (2018). Precursory slope distress prior to the 2010 Mount Meager landslide, British Columbia. *Landslides*, *15*(4), 637–647. https://doi.org/10.1007/s10346-017-0901-0

Rocscience. (2019). Dips (Version 5) Graphical and statistical analysis of orientation data [Software]. [Data Set]. *Rocscience, Inc*.

Smith, M. W., Carrivick, J. L., Hooke, J., & Kirkby, M. J. (2014). Reconstructing flash flood magnitudes using 'Structure-from-Motion': A rapid assessment tool. *Journal of Hydrology*, *519*, 1914–1927. https://doi.org/10.1016/j.jhydrol.2014.09.078

Staines, K. E., & Carrivick, J. L. (2015). Geomorphological impact and morphodynamic effects on flow conveyance of the 1999 jökulhlaup at Sólheimajökull, Iceland. *Earth Surface Processes and Landforms*, *40*, 1401–1416. https://doi.org/10.1002/esp.3750

Van Rijn, L. C. (1984). Sediment transport, Part I: Bed load transport. *Journal of Hydraulic Engineering*, *110*(10), 1431–1456. https://doi.org/10.1061/(ASCE)0733-9429(1984)110:10(1431)

Vasquez, J. A. (2017). *Modelling the generation and propagation of landslide-generated waves*.

Yin, Y. P., Huang, B., Chen, X., Liu, G., & Wang, S. (2015). Numerical analysis on wave generated by the Qianjiangping landslide in three gorges reservoir, China. *Landslides*, *12*(2), 355–364.